Preprints of the 21st IFAC World Congress (Virtual)
Berlin, Germany, July 12-17, 2020

# Observer Design for non-stationary oscillating Disturbances in Mixing Processes

**Patric Skalecki** * **Sonja Laicher** * **Mark Wörner** **
**Oliver Sawodny** *

* *Institute for System Dynamics, University of Stuttgart, Waldburgstr. 19, D-70563 Stuttgart.*
** *Liebherr-Mischtechnik GmbH, Im Elchgrund 12, D-88427 Bad Schussenried.*

**Abstract:** Information on the progression of the mixing process and quality are essential for mass concrete production. The power profile during the course of mixing can be used to evaluate the mixing process and its quality. Thus, a method for monitoring the average power transferred into the mixing material is presented, which enables an online mixture control based on the mechanical properties of the materials. An extensive experimental program on a 60 l laboratory twin-shaft mixer and a large-scale construction site mixer was performed to characterize mixer specific effects. For example, losses and speed dependent mixer shaft effects are examined. The portability and scalability of the results of the laboratory mixer is demonstrated by a comparison with a large construction site mixer. Based on the experimental insights, a signal model is derived which accounts for the characteristic disturbances in the power profile. Secondly, an extended Kalman filter is designed to estimate the disturbances online to separate these from the mean power signal, which can be used for evaluation of the concrete mixing progress. Finally, experimental results for different operating conditions and a comparison to classical signal filters such as a moving average filter and a low pass filter are presented, which show the increased performance of the presented approach.

*Keywords:* disturbance rejection, extended Kalman filters, signal reconstruction, industry application, mixing technology, twin-shaft mixer

## 1. INTRODUCTION

The world population is growing steadily with an expected increase of 2.6 billion people by 2050 (United Nations (2015)). This leads to rapid urbanization and the need of new housing and infrastructure. Likewise, the construction industry is steadily growing and thus the demand for high quality concrete is likely to increase. Hence a fast and reliable production process is required. Twin-shaft mixers are typically used for mass concrete production with high concrete discharge rates. Such mixing plants are able to produce more than $200\,\mathrm{m}^3/\mathrm{h}$. In order to guarantee a constant concrete quality, it is usually necessary to ensure workability. A common method for determining the concrete's quality is the concrete slump test. However, such tests have to be performed manually, which makes them impractical for supervising large amounts of concrete. Therefore, an online characterization of the concrete inside the mixer is desired. The supervision of the concrete mixing process is commonly done by monitoring the electrical power drawn from the grid. For example, Cazacliu and Roquet (2009) investigate the evolution of the mixing process and recipe changes in terms of the electrical power and its fluctuations. Dils et al. (2012) use power measurements to determine the power decay during mix evolution and a criteria for the optimal mixing time. More recently, Juez et al. (2017) study image analysis methods for determining the mixing evolution and use the mixing power consumption to validate their results.

The key idea in these studies is to characterize the mixing process in terms of the shear resistance evolution. More precisely, the transient shear resistance evolution is an indicator for the concrete's homogenization whereas the final shear resistance level determines its workability (Wallevik and Wallevik (2017)). This means that at a constant speed, the mechanical mixing power introduced into the mixture is the decisive quantity to determine the concrete quality. For this purpose, it is first necessary to infer the net mixing power from the overall input power. Secondly, it is desirable to split the power signal into its mean value and mixer characteristic effects. This has to be done with minimum information loss to preserve process-related disturbances. For further evaluation an online applicable method which is not limited to constant speed set points is required.

In the presented contribution we derive a simplified system model based on the principle of the angular momentum of a twin-shaft mixer. The losses are characterized via an identified characteristic curve and validated on experimental results. Further, we present a signal analysis in order to derive a signal model by means of which the

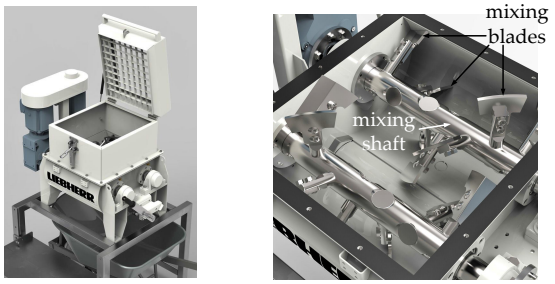


(a) Overview (b) Interior

Fig. 1. Scheme of the 60 l laboratory mixer (Liebherr-Mischtechnik GmbH (2019))

mechanical mixing torque can be tracked and divided. Thus an extended Kalman filter is designed for estimating all modeled states.

Section 2 describes the mixing system and introduces the system model including losses. The load torque is discussed in section 3 and the observer is designed. Section 4 presents the experimental results. Finally, concluding remarks and aspects of future work are given in section 5.

## 2. TWIN-SHAFT MIXER

For mass concrete production, a high discharge rate together with an insight into quality indicating parameters such as the shear resistance in the mixing plant are desirable. Twin-shaft mixers are commonly used in the industry to achieve high performance. These mixers consist of a mixing trunk and two mixing shafts driven by a coupled powertrain. Due to the large batch sizes of more than $5\,\mathrm{m}^3$, such mixers are impractical for analysis. Thus, a downsized version of the large construction site mixer is used for analysis. For this study a 60 l laboratory twin-shaft mixer provided by Liebherr-Mischtechnik GmbH is used, as depicted in Fig. 1. This mixer provides the same functionality and characteristics as the commercial one. Each shaft consists of seven blades with different shapes which are evenly distributed along the shaft at six radial positions and seven lateral positions. The shafts are operated by two 2.2 kW asynchronous motors (ASM) with a bevel gear box. Thus the operating speed range of the mixer shafts is between 20 and 110 rpm. To prevent a collision of the mixing blades the ASMs are synchronized with a toothed belt at drive side, which is mounted under the top cage on the motors in Fig. 1 (a). Both ASMs are operated by one common frequency converter (FC) in parallel.

In the experimental setup, the position of the ASMs is measured with two rotary encoders for each shaft at drive side. The FC provides electrical measurements for the motors such as active power, effective voltage, and current. In addition, the FC estimates the mechanical speed and torque on the drive side. This sensor information is not a standard feature of large mixing plants, but can easily be integrated. The only difference between the powertrain topology of the laboratory and the commercial mixer is a different energy conversion scheme and the use of a FC. As large-scale mixers are commonly operated at one speed, there is no need of a FC and the ASMs are directly operated on the 50 Hz grid. The energy is then transferred

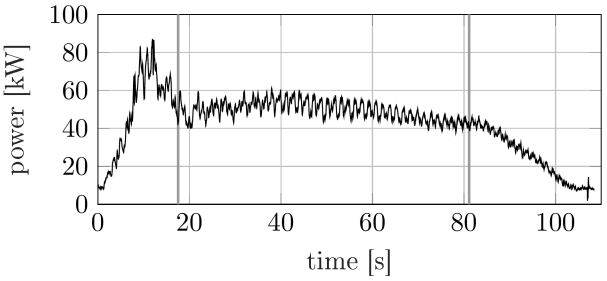


(a) Construction site mixer at 20 rpm

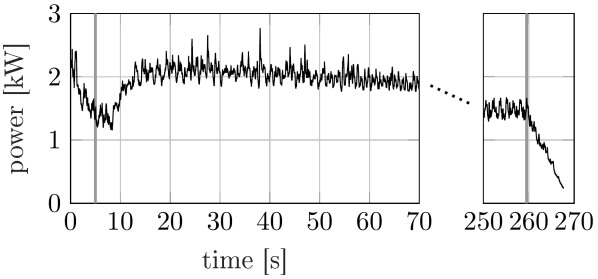


(b) Laboratory mixer at 40 rpm

Fig. 2. Active power during the production of a concrete batch.

to the mixing shaft via a belt drive on a synchronization joint shaft which couples the two planetary gear boxes.

For evaluation of the concrete mixing process, the electrical power drawn from the grid is investigated. A typical power profile during the production of a $2.5\,\mathrm{m}^3$ concrete batch is displayed in Fig. 2 (a). The mixing process consists of the three different production stages *feeding*, *mixing*, and *discharging* as described in Deligiannis and Manesis (2008). The gray vertical lines denote state changes. During feeding, the solid raw materials are fed into the mixer causing an initial increase of the power. As soon as water is added the power demand begins to decrease. The mixing stage begins after all ingredients have been filled into the mixing chamber. A typical power increase is observed at first, which slowly decreases afterwards until it settles to an almost constant value before discharge. The same pattern can be recognized in the power profile of the laboratory mixer in Fig. 2 (b). The mixer is preloaded with all dry raw materials and the water is added at time zero where the mixing speed is at 40 rpm. Thus, the initial power increase during the feeding process does not occur as seen for the large-scale mixer during the first 10 s. Due to the design of the mixing shaft and the uneven distribution and shape of the mixing blades, oscillations superimpose the power signal. Each time a mixing blade dips into or leaves the material the power consumption changes. The stronger signal-to-noise ratio for the laboratory mixer is due to the downscaling, since the gravel size remains constant within the concrete, which disturbs the large mixing plant less. This effect is also amplified by the use of a speed controlled FC reacting on speed disturbances due to the mixer characteristics and coarse aggregates. However, these oscillations are systematic and depend e.g. on the mixing speed, the mixer design and the filling level. This enables a derivation of a dynamic signal model in order to reconstruct the original power profile by a model-based state observer. With the ability

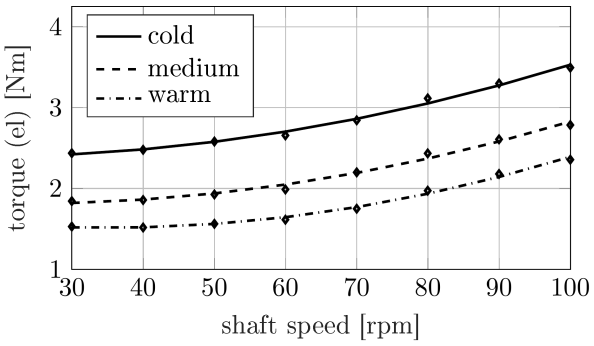


Fig. 3. Loss characteristic at different operating states.

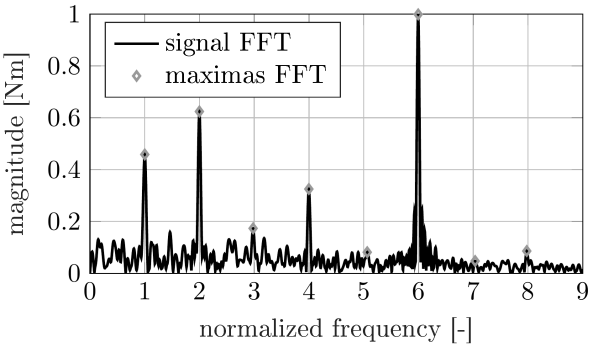


Fig. 4. Normalized frequency spectrum of the torque signal for 60 l filling level and 80 rpm mixing shaft speed.

of separating different dynamics, represented by different model states, the disturbance-free signal can be extracted and used for the analysis of the mixing process and the mixing quality. It is therefore a key parameter for the evaluation of new control schemes.

### *2.1 System model*

A simplified model is derived to capture the dominant system behavior for the observer and due to the limited sensor information. Assuming that the system is sufficiently stiff it can be regarded as one big shaft transformed to the drive side. Consider the principle of angular momentum

$$J\dot{\omega} = M, \tag{1}$$

where $J$ is the overall inertia, $\omega$ the rotational speed and $M$ the effective torque at drive side. In this case, the overall inertia

$$J = 2\left(J_\mathrm{r} + \frac{1}{\eta_\mathrm{g} i^2}(J_\mathrm{g} + J_\mathrm{s})\right) \tag{2}$$

is the sum of the drive rotor $J_\mathrm{r}$, the gear box $J_\mathrm{g}$, and the shaft $J_\mathrm{s}$. The latter two are transformed to the drive side by the gear ratio $i$ and the efficiency $\eta_\mathrm{g}$. The effective torque is the sum of all torques

$$M = M_\mathrm{el} - M_\mathrm{loss} - M_\mathrm{load}, \tag{3}$$

where $M_\mathrm{el}$ is the torque generated by the ASMs, $M_\mathrm{load}$ is the torque generated by the mixing material on the shafts and $M_\mathrm{loss}$ covers other losses such as friction and electrical losses. Various experiments at different operating speeds have shown that the losses can be modeled as a quadratic characteristic curve in the rotational speed

$$M_\mathrm{loss}(\omega) = c_0 + c_1\omega + c_2\omega^2, \tag{4}$$

where $c_0$ to $c_2$ are parameters for identification. These parameters depend on the operating states since changes in gear oil and motor temperature affect the losses of the system. This effect is shown in Fig. 3. The markers are generated by operating the mixer at the given speed and averaging the recorded torque. The three lines are a least squares fit for the loss curve at the operating states ranging from a cold system to a system at desired operating temperature (warm).

By inserting the equations into (1), the state-space notation

$$\dot{x}_\mathrm{sys} = \begin{bmatrix} x_{\mathrm{sys},2} \\ \frac{1}{J}\left(M_\mathrm{el} - M_\mathrm{loss}\left(x_{\mathrm{sys},2}\right) - M_\mathrm{load}\right) \end{bmatrix} \tag{5}$$

is derived, where the state

$$x_\mathrm{sys} = \begin{bmatrix} \varphi \\ \omega \end{bmatrix} \tag{6}$$

comprises the angle $\varphi$ and angular speed $\omega$ of the motor. Note that the loss characteristic is quadratic and thus a nonlinear function.

## 3. DESIGN OF THE LOAD OBSERVER

In order to obtain measurements free of oscillations caused by the mixer characteristics, a filter needs to be designed to split the torque signal into the mean and the oscillation prediction. Classical signal filters will lead to a delayed reaction if applied online and cannot account for dynamic changes and losses. In particular, commonly used low-pass filters eliminate all dynamics higher than the cutoff frequency and not just these relevant for the disturbances due to the mixing blades. Therefore, an extended Kalman filter (EKF) is used similar to the approach presented by Zimmert and Sawodny (2008).

First, the signal analysis for identification of the mixer characteristics is discussed. Then the signal model for tracking the real torque measurements is derived. An EKF is used as observer for the nonlinear system and signal model.

### *3.1 Signal analysis*

The mixer characteristics need to be analyzed to design a signal model to track the torque signal. Thus, an experimental program for evaluating the influence of shaft speed and filling level is conducted. Wet sand is used as mixing material to cancel out transient behavior of the material during the mixing process and thus capture the mixer characteristics. This program consists of eight constant speed levels ranging from 30 to 100 rpm and ten different filling levels ranging from 10 to 100 l representing a test grid for load use cases. Considering the mean-free frequency spectrum of the torque signal at 80 rpm shaft speed and 60 l volume of material, it can be seen, that the signal can be approximated by a sum of sinusoidal functions with the same frequency as the mixing shaft and its multiples. Fig. 4 shows this spectrum, where the frequency axis is normalized by the mixing shaft frequency. The gray diamonds are the local maxima around the multiples. A collection of all maxima in the frequency spectrum over the whole experimental program is visualized in Fig. 5 (a). Due to the maximization of the peak magnitude around the integer normalized frequencies two different patterns arise. The first can be observed at the

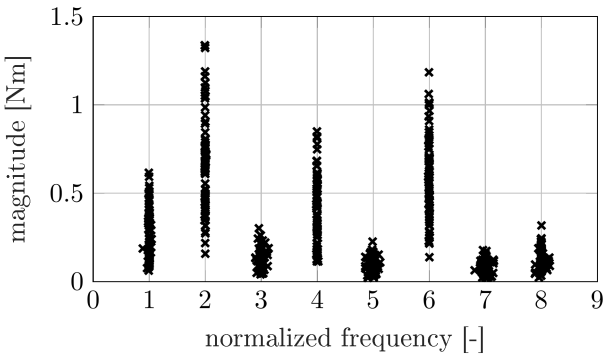


(a) Laboratory mixer over the experimental program.

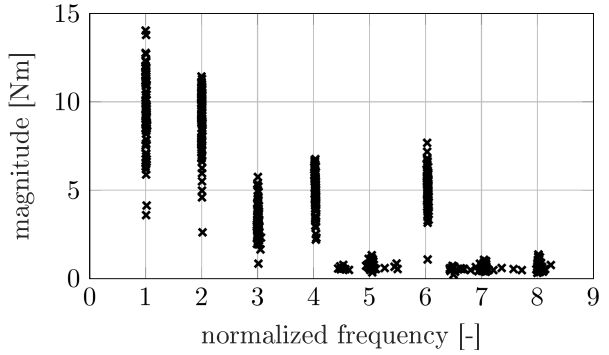


(b) Construction site mixer at constant speed.

Fig. 5. Maxima in the frequency spectrum.

normalized frequencies 3, 5, 7, and 8, where the magnitude and its variation is small, but the variation in normalized frequencies is large. The frequency variation and the low impact of the magnitude show that this pattern is not well suited for signal reconstruction. The second pattern can be observed at normalized frequencies 1, 2, 4, and 6. The magnitude is significantly higher than at the other frequencies. Although also the magnitude variation is increased, the magnitude peaks are observed exactly at the normalized frequencies. Hence, this pattern and, therefore, these normalized frequencies represent the most dominant mixer characteristics. The variations in magnitude can be handled by the observer.

A normalized frequency spectrum for the large-scale mixing process of 100 concrete batches is shown in Fig. 5 (b). The batches are produced on a large construction site mixer operated at constant speed and mixed directly one after the other with the same concrete recipe. The large variations in magnitude can be explained by filling level variations. The dominant normalized frequencies for this mixer differ slightly since the mixing shafts show small differences to the laboratory mixer. However, both mixers share the structure of seven blades at six radial positions. A possible interpretation for this is that the first normalized frequency (shaft speed) corresponds to the radial position with two blades compared to all others and normalized frequency 6 appears because there are six radial positions. The impact of integer normalized frequencies between 2 and 5 vary depending on the shaft and blade design and how the two mixing shafts are positioned to each other. This behavior could also be observed at the laboratory mixer for a different mixing shaft design. Therefore, the general mixer characteristics between the different mixer scales are comparable which justifies the scalability.

### *3.2 Signal Model*

As shown in the previous section, the torque signal can be expressed by a constant or slowly changing part and a sum of sinusoidal functions, where the frequency is the mixing shaft frequency and its multiples. Therefore, the signal model for an EKF needs to capture these dynamics. The slowly changing dynamics for tracking the signal's mean value is modeled by

$$\dot{x}_\mathrm{c} = 0 \tag{7}$$

and thus assuming the state $x_\mathrm{c}$ to be constant. The sinusoidal part $x_{\sim,m}$ is expressed by the standard oscillation model

$$\dot{x}_{\sim,m} = \begin{bmatrix} 0 & 1 \\ -m^2\omega_\mathrm{S}^2 & 0 \end{bmatrix} x_{\sim,m} = A_{\sim,m}(\omega_\mathrm{S}) x_{\sim,m}, \tag{8}$$

where $\omega_\mathrm{S}$ is the shaft frequency, $m$ is a factor for its multiples and the subscript $\sim$ is used to describe the oscillation states. The combination of all models for the aforementioned four dominant frequencies results in a nine dimensional state space with the state vector

$$x_\mathrm{load} = \begin{bmatrix} x_\mathrm{c} & x_{\sim,1}^\top & x_{\sim,2}^\top & x_{\sim,4}^\top & x_{\sim,6}^\top \end{bmatrix}^\top \tag{9}$$

and the dynamic matrix

$$A_\mathrm{load}(\omega_\mathrm{S}) = \mathrm{diag}\left(0,\ A_{\sim,1},\ A_{\sim,2},\ A_{\sim,4},\ A_{\sim,6}\right). \tag{10}$$

The relationship

$$M_\mathrm{load} = [1\ 1\ 0\ 1\ 0\ 1\ 0\ 1\ 0]\, x_\mathrm{load} = c_\mathrm{load}^\top x_\mathrm{load} \tag{11}$$

is used as a connection to reconstruct the measured torque signal generated by the mixture. Hence, the resulting overall linear system for the mixer characteristics and load is

$$\begin{aligned} \dot{x}_\mathrm{load} &= A_\mathrm{load}(\omega_\mathrm{S}) x_\mathrm{load} \\ M_\mathrm{load} &= c_\mathrm{load}^\top x_\mathrm{load}. \end{aligned} \tag{12}$$

### *3.3 Load Observer*

To split the signal into a non-oscillating and an oscillating part, the previous signal model is incorporated into an EKF. Therefore, the state space is extended to

$$x = \begin{bmatrix} x_\mathrm{sys} \\ x_\mathrm{load} \end{bmatrix}. \tag{13}$$

The combined system

$$\dot{x} = f(x,u) = \begin{bmatrix} x_2 \\ J^{-1}\left(u - M_\mathrm{loss}(x_2) - \begin{bmatrix} 0 & c_\mathrm{load}^\top \end{bmatrix} x\right) \\ \begin{bmatrix} 0 & A_\mathrm{load}(i^{-1}x_2) \end{bmatrix} x \end{bmatrix} \tag{14}$$

follows by using the load torque $M_\mathrm{load} = \begin{bmatrix} 0 & c_\mathrm{load}^\top \end{bmatrix} x$ and the rotational speed of the mixer shaft $\omega_\mathrm{S} = i^{-1}x_2$. The system input $u$ is the measured electrical torque $M_\mathrm{el}$, which is captured by the FC. The angular position

$$y = c^\top x = x_1 \tag{15}$$

is used as output for the EKF model. The local observability matrix

$$O = \begin{bmatrix} c^\top & c^\top A & c^\top A^2 & \dots & c^\top A^{10} \end{bmatrix}^\top \tag{16}$$

has a full rank of 11, where the system matrix $A$ is the linearization

$$A = \frac{\partial}{\partial x} f(x,u)|_{x=x_s} \tag{17}$$

around an arbitrary state vector $x_s$. This shows that the setup is locally feasible for a given frequency.

The weighting matrices $Q$ for the process noise and $R$ for the measurement noise need to be selected within the filter design. The matrix $Q$ is set to a diagonal structure because the components of each signal part in the signal model can be seen as independent of each other and of the system dynamics. The weighting parameters of the oscillating signal model parts are all set to the same value for all four frequencies. Thus the total number of design parameters

$$\begin{aligned} Q &= \mathrm{diag}\left(q_\omega, q_{\dot{\omega}}, q_c, q_\sim, \ldots, q_\sim\right) \\ R &= r \end{aligned} \tag{18}$$

is reduced to five free parameters. The parameter $q_{\dot{\omega}}$ can be approximated based on the signal variance of the input $u$ of measurements when interpreted as additive input noise.

## 4. EXPERIMENTAL RESULTS AND DISCUSSION

In order to evaluate the performance of the proposed EKF, the free parameters (18) were adjusted offline in simulations using the measurement data obtained during the experimental program. Next, the EKF is applied to an online setup and compared to classical signal filters. For online evaluation of the mean mixing power, the EKF needs to satisfy the criteria

(1) to enable a precise and fast separation of the mean and oscillation part of the torque signal,
(2) and to show a smooth and fast tracking of the speed signal.

These criteria ensure a smooth mean mixing power signal, which could be used for online quality estimation and control of the batch. For practical reasons it is desired to have one parameter set for all operating points regarding speed and filling level. This eliminates the need for calibration or switching before new experiments are conducted. The first criteria translates to the weights, where the constant weight $q_c$ should be small compared to the frequency weight $q_\sim$. This ensures, that small deviations due to noise are captured by the oscillation model and not by the mean prediction. The process weight $q_\omega$ and the measurement weight $r$ need to be chosen relatively small in order to suppress the estimation of torque measurement noise and modeling errors into the speed signal. Finally, the weight for the process noise $q_{\dot{\omega}}$ is selected such that the relative mean squared error (rel. MSE) is minimized. This iterative procedure resulted in a value close to the aforementioned method based on the interpretation as additive input noise. The MSE is computed between the raw torque signal $M_\mathrm{el}$ and the estimated load torque $M_\mathrm{load}$ corrected by the losses $M_\mathrm{loss}$. The different filling levels change the mean torque generated by the load significantly compared to speed changes. Thus, the MSE is normalized by the mean torque over all experiments with the same filling level $\bar{M}_\mathrm{el}$. The rel. MSE is defined as

$$\text{rel. MSE} = \frac{1}{N\bar{M}_\mathrm{el}} \sum_{k=0}^{N-1} (M_{\mathrm{el},k} - M_{\mathrm{load},k} - M_{\mathrm{loss},k})^2, \tag{19}$$

where the subscript $k$ denotes the time step index. The rel. MSE is calculated over all different speed levels since these are incorporated in the signal model and impact the rel. MSE less than the filling level. The calculated error values are given in table 1 for different filling levels. The MSE increases with a higher filling level due to the larger torque amount needed for more mixing material. The rel. MSE initially increases, culminates at 40 l and decreases again. This behavior is independent from the choice of the observer parameters and could be a result of the material-mixer interaction based on the filling level.

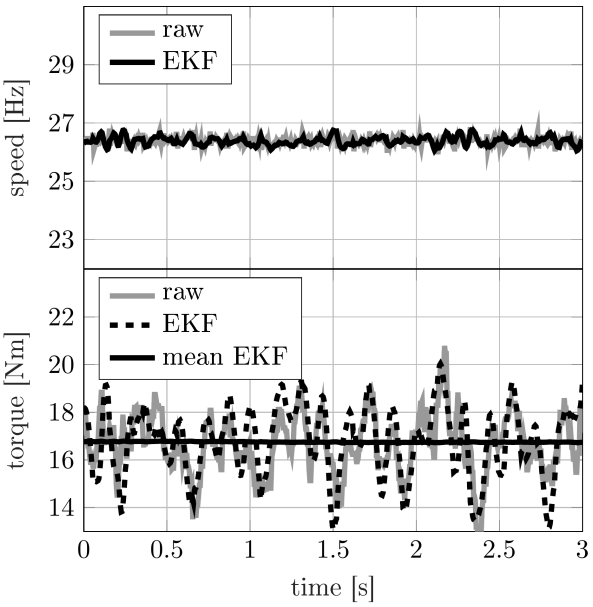


Fig. 6. Tracking the mixing speed and torque at drive side and by the loss $M_\mathrm{loss}$ corrected EKF prediction.

Table 1: Errors on the experimental program.

| volume [l] | MSE [Nm] | mean [Nm] | rel. MSE [%] |
|---|---|---|---|
| 10 | 0.26 | 4.24 | 6.1 |
| 20 | 0.39 | 5.02 | 7.8 |
| 30 | 0.50 | 6.05 | 8.3 |
| 40 | 0.79 | 7.53 | 10.5 |
| 50 | 0.94 | 9.04 | 10.4 |
| 60 | 1.04 | 11.04 | 9.4 |
| 70 | 1.20 | 13.55 | 8.8 |
| 80 | 1.47 | 16.76 | 8.8 |
| 90 | 1.92 | 20.67 | 9.3 |
| 100 | 1.81 | 23.63 | 7.7 |

For evaluation of the tracking performance, a 3 s segment is shown in Fig. 6, where the mixer has been loaded with 80 l wet sand and is operated at 70 rpm. Here, the predicted torque is corrected by the loss $M_\mathrm{loss}$. The scaling of the $y$-axis in Fig. 6 is selected such that they are comparable regrading the magnitude. The raw speed signal is constructed by numerical differentiation of the encoders and the periodic spikes resulted from the speed controller and the periodic mixer characteristic. The recorded mixer signals are displayed in gray and the EKF reconstruction in black. The EKF is able to accurately predict the course of the speed and the torque signal. With the selected design parameters, a slight damping of the spikes is observed for the EKF in speed signal. The torque signal of the EKF is displayed for the estimated mean torque (solid line) and the mean torque superimposed by the disturbances (dashed line). The EKF is able to estimate and eliminate

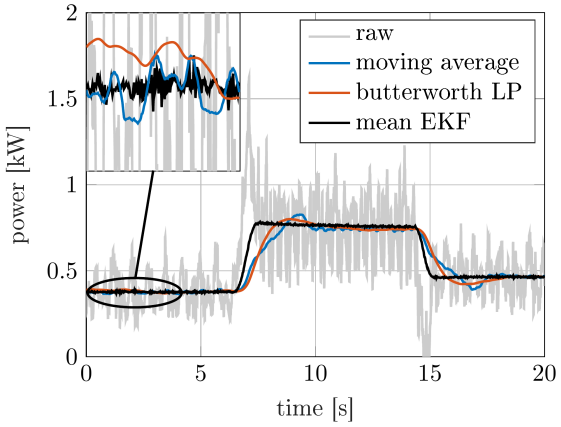


Fig. 7. Comparison of the proposed EKF to a moving average and butterworth low-pass filter.

the disturbances, which demonstrates that modeling the four dominant frequencies is sufficient for signal reconstruction.

The dynamic tracking capabilities of the observer are investigated using setpoint changes. In this case, steep speed ramps of different magnitudes were applied, where the power will increase to accelerate the shaft. A moving average filter and a butterworth low pass filter were designed to compare the EKF performance. The results of the three filters are shown in Fig. 7, where the mixer was loaded with 50 l wet sand and the speed was increased from initially 40 rpm to 80 rpm before slowing down to 50 rpm. The raw power data subtracted by the identified loss curve is visualized in gray. Power peaks due to shaft acceleration and deceleration are included and need to be handled by the filters. The results of the two signal filters are displayed in blue and red. Since the relevant frequencies to be filtered out are relatively small (below 0.33 Hz), both filters have to be designed sufficiently slow and with a distinct cutoff frequency. This leads to high phase shifts during setpoint changes. In addition, the cutoff frequencies of the filters must either be redesigned for each speed or the filter performance worsens. Reconstructing the mixing power based on the mean EKF prediction results in a accurate and almost delay- free tracking of the setpoint change. The power required for the acceleration and deceleration of the shaft is effectively filtered out by the EKF. This can be observed during the setpoint change, where the EKF prediction does not overshoot and increases and decreases more slowly than the raw signal. The enlarged snippet in Fig. 2 highlights the tracking performance during the first 3 s. It can be observed that both signal filters do not track the mean steadily. The mean prediction of the EKF is able to eliminate the disturbances although the mean is superimposed by high frequency oscillations due to the artifacts in the speed estimation.

## 5. CONCLUSION

The power profile of a mixer during operation can be correlated to the evolution of the concrete mixing process and is thus an indicator of the homogenization level of the concrete. To detect small changes in the power profile, disturbances which are not due to material changes, for example oscillations introduced into the signal by the mixing paddles, need to be detected and eliminated. An extensive test program is therefore conducted to model these effects. It is shown that these disturbances result from periodic effects and can be modeled using an oscillation model. Methods are derived on a 60 l laboratory twin-shaft mixer and shown to be comparable and transferable to large-scale construction site mixing plants. Systematic errors, for example due to speed-dependent losses, are incorporated. Since the characteristic of the mechanical mixing power needs to be known online during the mixing process, an EKF is designed which tracks the oscillations online considering speed and load changes. In comparison to standard filter schemes, the EKF is able to accurately identify the oscillation frequencies, to maintain the general characteristics of the power profile, and react to setpoint changes with almost no delay.

As a next step, the disturbance-free power signal can be used to observe and estimate the quality and homogenization level of the concrete directly during mixing. In addition, the proposed method can be expanded to other mixer designs, which often suffer from periodic disturbances due to the uneven design of the mixing shaft and mixing paddles.

## REFERENCES

Cazacliu, B. and Roquet, N. (2009). Concrete mixing kinetics by means of power measurement. *Cement and Concrete Research*, 39(3), 182 – 194. doi:https://doi.org/10.1016/j.cemconres.2008.12.005.

Deligiannis, V. and Manesis, S. (2008). Concrete batching and mixing plants: A new modeling and control approach based on global automata. *Automation in Construction*, 17(4), 368 – 376. doi:https://doi.org/10.1016/j.autcon.2007.06.001.

Dils, J., Schutter, G.D., and Boel, V. (2012). Influence of mixing procedure and mixer type on fresh and hardened properties of concrete: a review. *Materials and Structures*, 45(11), 1673–1683. doi:10.1617/s11527-012-9864-8.

Juez, J.M., Artoni, R., and Cazacliu, B. (2017). Monitoring of concrete mixing evolution using image analysis. *Powder Technology*, 305, 477–487. doi:10.1016/j.powtec.2016.10.008.

Liebherr-Mischtechnik GmbH (2019). Data sheet for twin-shaft laboratory mixer DW 0.06/100. `https://www.liebherr.com/en/deu/products/construction-machines/concrete-technology/mixer-systems/laboratory-mixer/details/325083.html`. [Online; accessed 11/08/2019].

United Nations (2015). World Urbanization Prospects: The 2014 Revision. Technical report, United Nations, Department of Economic and Social Affairs, Population Division.

Wallevik, J.E. and Wallevik, O.H. (2017). Analysis of shear rate inside a concrete truck mixer. *Cement and Concrete Research*, 95, 9–17. doi:10.1016/j.cemconres.2017.02.007.

Zimmert, N. and Sawodny, O. (2008). A trajectory tracking control with disturbance-observer of a fire-rescue turntable ladder. In *2008 American Control Conference*. IEEE. doi:10.1109/acc.2008.4587125.